Hinge-Free Compliant Mechanism Design via the Topological Level-Set

Anirudh Krishnakumar, Krishnan Suresh

suresh@engr.wisc.edu

Department of Mechanical Engineering

UW-Madison, Madison, Wisconsin 53706, USA

ABSTRACT

The objective of this paper is to introduce and demonstrate a new method for the topology optimization of compliant mechanisms. The proposed method relies on exploiting the topological derivative, and exhibits numerous desirable properties including: (1) the mechanisms are hinge-free, (2) mechanisms with different geometric and mechanical advantages can be generated by varying a single control parameter, (3) a target volume fraction need not be specified; instead numerous designs, of decreasing volume fractions, are generated in a single optimization run, and (4) the underlying finite element stiffness matrices are well-conditioned. The proposed method and implementation are illustrated through numerical experiments in 2D and 3D.

1. INTRODUCTION

Compliant mechanisms are popular in mechanical design for multiple reasons: they are easy to fabricate, exhibit low wear and low friction, and have a built-in restoring force [1], [2]. They are often preferred over their rigid-body counterparts in various applications including micro-electro-mechanical-systems (MEMS) [3], surgery [4], torque-measurements [5], etc.

Compliant mechanisms are synthesized today through one of two distinct methods [6]: (1) pseudo rigid body models, and (2) topology optimization. The relative advantages of these two methods are discussed, for example, in [6], [7]. The focus of this paper is on topology optimization of compliant mechanisms.

Topology optimization of compliant mechanisms entails two tasks: (1) *Design formulation*: How does one formulate and pose the design problem of compliant mechanisms, i.e., how does one prioritize various objectives such as flexibility, stiffness, and efficiency? (2) *Spatial parameterization*: How does one parameterize the spatial domain to solve the design problem?

Various design formulations and spatial parameterization techniques have been proposed; these are reviewed in Section 2. Typically, any combination of the two can be chosen; however, certain pairs have been established to be robust and efficient.

In this paper, a specific combination of design formulation and spatial parameterization method is considered; this combination relies heavily on the concept of topological derivative rather than pseudo-densities used in Solid Isotropic Material with Penalization (SIMP). By avoiding pseudo-densities, many of the 'hinge-problems' are avoided; see, for example, [8], [9]. The proposed methodology is established in Section 3, while the implementation details are discussed in Section 4. This is followed by numerical experiments in Section 5, and conclusions in Section 6.

2. LITERATURE REVIEW

Consider the 'classic inverter' problem posed in Figure 1: a force is applied on one side, and an 'inverted' output displacement is desired on the other side. A suitable compliant mechanism must be designed within the specified domain to achieve this objective.

As is well known, this entails multiple objectives [10], [11], [12], [13], [14]: (1) the compliant mechanism must exhibit *sufficient flexibility* to achieve the desired displacement at the output, and (2) it must exhibit *sufficient stiffness* to resist a work-piece at the output. In addition, constraints on the input displacement, and maximum stress constraints must be met. Finally, it is desirable to avoid 'hinges' and 'checker-board patterns'.

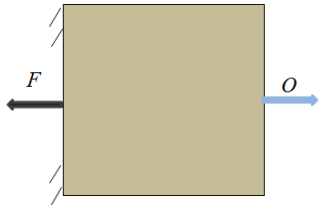

Figure 1: Classic inverter problem.

Flexibility of a compliant mechanism is usually quantified via one of the following: (a) as the ratio of output to input displacement, i.e., geometric advantage [15], or (b) the mutual strain energy [10], [11], [16]. On the other hand, stiffness is usually quantified as: (a) the ratio of output to input force, i.e., mechanical advantage [12], or (b) output strain energy, or (c) the sum of input and output compliances [16]. Often, an auxiliary spring is used at the output to capture stiffness. Further, geometric and mechanical advantages can be combined into a single quantity namely transfer-efficiency [15], [17], [18].

Flexibility and stiffness typically work against each other. Consequently, compliant mechanism design is a multi-objective problem with multiple 'Pareto' solutions [2], [14]. For a given volume fraction, multiple solutions to the inverter problem exists [15], depending on how the two objectives are combined. For example, in [12], the mechanical advantage is maximized subject to flexibility constraints, whereas in [11], the ratio of mutual strain energy to output strain energy is maximized, etc. The relationship between many of these formulations is discussed in [12]. More recently, a metric to quantify the uniformity of the strain energy distribution within a compliant mechanism is proposed in [19]. Formulations that account for large displacements are considered in [17], [18], while cellular (repetitive) mechanisms are considered in [20] . A full summary of all such design formulations is beyond the scope of this paper; the reader is referred to [7], [21] for a review.

Once an appropriate combination of flexibility and stiffness has been chosen, a spatial parameterization technique is essential for optimization. By far, the most popular technique today is Solid Isotropic Material with Penalization (SIMP) [22], [23]. In SIMP, pseudo-densities are assigned to each of the finite-elements within the mesh, and optimized to result in a desired topology. Alternately, one may use level-sets [24], and these offer certain benefits over SIMP-based methods, summarized in [13], [17], [25], [26]. In addition, evolutionary methods [16], [27], ground structure methods [28] and homogenization methods [2] have also been explored.

Avoiding hinges in compliant mechanisms is of significant interest since hinges are regions of high stress concentration [8]. As explained in [8], there is an underlying (numerical) reason for the formation of hinges in SIMP-based topology optimization. To quote [8]: "*The conclusion then is that optimization algorithms are exploiting a loophole in the finite element model and the [SIMP-based] design parameterization of topology optimization to best optimize the objective function {to result in point flexures]*". In other words, since one is trying to maximize stiffness and output displacement, (finite) elements with low pseudo-densities create a 'loop-hole' for flexures to form: these flexures offer artificial finite stiffness with large output displacement. The authors of [8] therefore propose a novel scheme of penalizing the formation of such hinges. In [9], the authors suggest that one should maximize the strain energy stored in a mechanism, subject to input and output displacement constraints. In [15], the authors make use of multiple springs to achieve a hinge-free design. In this paper, by exploiting topological sensitivity instead of pseudo-densities, we directly avoid the formation of flexures. As a final note, the author of [29] provides an elegant method to detect and remove checker-board patterns during topology optimization.

The design formulation and spatial parameterization technique are typically independent of each other. However, together they determine the robustness, numerical efficiency, and simplicity of the resulting topology optimization method.

3. THEORY

In this paper, a specific combination of a design formulation and spatial parameterization technique is proposed. As discussed below, the design formulation is a modified version of the one proposed in [27], while the parameterization technique is a novel use of the topological sensitivity to compliant mechanism design.

3.1 Design Formulation

The proposed design formulation is illustrated using the inverter problem as an example. It is well known that this problem entails (repeated) solution of a pair of structural problems; the first is the 'input' problem where the force is applied as in Figure 2, resulting in the displacement field u_{in}, and the input strain energy:

$$S_{in} = \frac{1}{2}\int_{\Omega} \sigma(u_{in})\varepsilon(u_{in})d\Omega \tag{3.1}$$

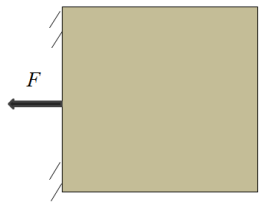

Figure 2: The primary input problem.

Next, a unit output force is applied as in Figure 3, resulting in the displacement field u_{out}, and the output strain energy:

$$S_{out} = \frac{1}{2}\int_{\Omega} \sigma(u_{out})\varepsilon(u_{out})d\Omega \tag{3.2}$$

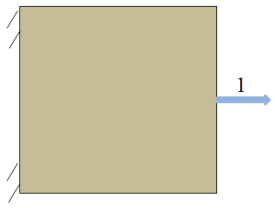

Figure 3: The secondary output problem.

Finally, given the two displacement fields, one can also define the mutual potential energy [30] as:

$$S_{mut} = \int_{\Omega} \sigma(u_{out})\varepsilon(u_{in})d\Omega \tag{3.3}$$

Various combinations of these three energies have been used to construct a design objective of compliant mechanisms (see [10], [21], [27]). In this paper, we start with the formulation proposed in [27]:

$$\begin{aligned} &Max\left(\varphi \equiv \frac{S_{mut}}{S_{in} + S_{out}}\right) \\ &v \le v_{\max} \end{aligned} \tag{3.4}$$

The motivations for the above definition are as explained in [27]: (1) the objective is non-dimensional, (2) external springs are not required, and (3) input and output displacement constraints are accounted for indirectly.

However, we propose a simple modification to the above objective, namely:

$$\begin{aligned} &Max\left(\varphi \equiv \frac{S_{mut}}{2\eta S_{in} + 2(1-\eta)S_{out}}\right) \\ &v \le v_{\max} \end{aligned} \tag{3.5}$$

where $0 < \eta < 1$ is a user-specified control parameter. Clearly, $\eta = 0.5$ recovers the original formulation. Later in the paper, we demonstrate that increasing η increases the geometric advantage, and decreases the mechanical advantage of the mechanism (and vice-versa). Given the above design formulation, the specific spatial discretization technique is discussed next.

3.2 Topological Derivative

The proposed technique relies heavily on the concept of topological derivative. Topological derivative, a.k.a., topological sensitivity, is the first order impact of inserting an infinitesimal hole on various quantities of interest. This concept has its roots in the influential paper by Eschenauer [31], and has later been extended and explored by numerous authors [32], [33], [34], [35], [36], including generalization to arbitrary features [37], [38], [39].

To understand this concept, consider again the inverter problem; let S denote any one of the energies defined earlier. Suppose we modify the topology by inserting a hypothetical hole of radius r at point p (see Figure 4). This insertion will result in a change in the quantity

S . Topological sensitivity is defined as the ratio of change in the quantity of interest to the area of the hole, as the hole-size is shrunk to zero. In 2-D, we have:

$$\mathcal{T}(p) \equiv \lim_{r \to 0} \frac{S(r) - S}{\pi r^2} \tag{3.6}$$

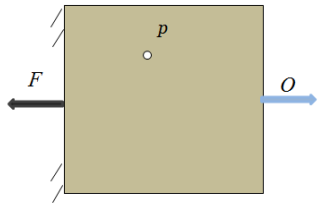

Figure 4: A hypothetical topological change.

Various strategies have been proposed to obtain a closed-form expression for the topological derivative. A particularly powerful strategy relates topological sensitivity to shape sensitivity [40]. Specifically, consider the problem posed in Figure 5, where the radius of the hole is controlled by a shape parameter τ .

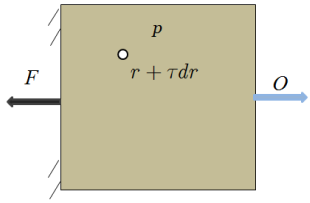

Figure 5: A hypothetical shape change.

For a given radius, one can define shape sensitivity as:

$$\chi(r) = \left. \frac{dS(r)}{dr} \right|_{r=0} \tag{3.7}$$

Well-known adjoint methods [41], [42], [43] can now be used to find closed-form expressions for shape-sensitivity (as a function of the radius r). It was established in [40] that topological derivative as defined in Equation (3.6) is related to shape sensitivity via:

$$\mathcal{T}(p) = \lim_{r \to 0} \frac{\chi(r)}{2\pi r} \tag{3.8}$$

Consequently, one can derive a closed-form expression for the topological derivative, and is given by [32], [33], [34], [35], [36]:

$$\mathcal{T}(p) = \frac{4}{1+\nu} \sigma(u) : \varepsilon(\lambda) - \frac{1-3\nu}{1-\nu^2} tr(\sigma(u)) tr(\varepsilon(\lambda)) \tag{3.9}$$

where ν is the Poisson ratio, $\sigma(u)$ is the stress field associated with the primary field u, and $\varepsilon(\lambda)$ is the strain field associated with an adjoint field λ (see next Section). The stresses and strains are evaluated at point p *in the original domain, i.e., before the hole is inserted*.

In 3-D, the topological sensitivity field is given by:

$$\mathcal{T} = 20\mu\sigma(u) : \varepsilon(\lambda) + (3\gamma - 2\mu) tr\sigma(u) tr\varepsilon(\lambda) \tag{3.10}$$

where $\mu \,\&\, \gamma$ are the Lame parameters.

3.3 Topological Fields

The objective posed in Equation (3.5) involves three quantities of interest: S_{in}, S_{out} & S_{mut}. One can therefore define three topological sensitivities. Specifically, if we set $S = S_{in}$, then one can show that the adjoint is $\lambda = -u_{in}$ (see [40], for example); therefore, in 2-D:

$$\mathcal{T}_{in}(p) = -\frac{4}{1+\nu}\sigma(u_{in}) : \varepsilon(u_{in}) + \frac{1-3\nu}{1-\nu^2} tr\left[\sigma(u_{in})\right] tr\left[\varepsilon(u_{in})\right] \tag{3.11}$$

Similarly, with $S = S_{out}$, we have $\lambda = -u_{out}$:

$$\mathcal{T}_{out}(p) = -\frac{4}{1+\nu}\sigma(u_{out}) : \varepsilon(u_{out}) + \frac{1-3\nu}{1-\nu^2} tr\left[\sigma(u_{out})\right] tr\left[\varepsilon(u_{out})\right] \tag{3.12}$$

Finally, $S = S_{mut}$ we have:

$$\mathcal{T}_{mut}(p) = -\frac{4}{1+\nu}\sigma(u_{in}) : \varepsilon(u_{out}) + \frac{1-3\nu}{1-\nu^2} tr\left[\sigma(u_{in})\right] tr\left[\varepsilon(u_{out})\right] \tag{3.13}$$

In other words, given the two displacement fields in the original domain (without the hole), one can compute the topological sensitivities for the three quantities; these are illustrated in Figure 6 (scaled for convenience).

Figure 6a, for example, illustrates the *input* topological sensitivity: observe that inserting a hole near the point of force application or near the displacement constraint has a significant impact on input strain energy (as expected), whereas inserting a hole far away from these locations has little or no impact. The other two fields can be interpreted similarly; the mutual topological sensitivity field is 'flat', and often difficult to visualize.

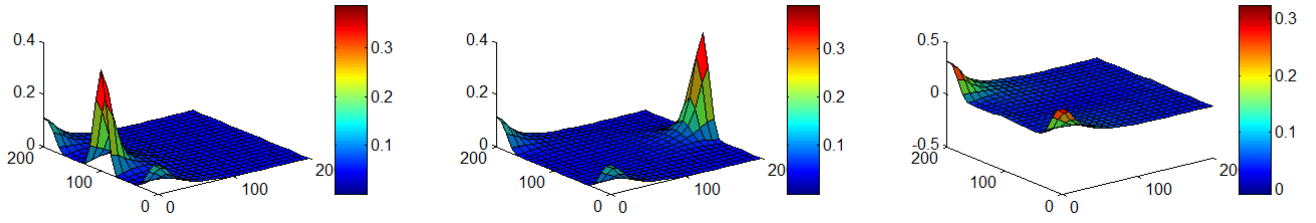

(a) Input topological sensitivity. (b) Output topological sensitivity. (c) Mutual topological sensitivity.

Figure 6: The three topological sensitivity fields.

Given these three fields, one can compute the topological sensitivity of the objective function φ by differentiating Equation (3.5) and applying the chain rule, resulting in:

$$\mathcal{T}_{\varphi} = w_{mut}\mathcal{T}_{mut} - (w_{in}\mathcal{T}_{in} + w_{out}\mathcal{T}_{out}) \tag{3.14}$$

where the weights are given by:

$$\begin{aligned} w_{in} &= \frac{2\eta S_{mut}}{\left(2\eta S_{in} + 2(1-\eta)S_{out}\right)^2} \\ w_{out} &= \frac{2(1-\eta)S_{mut}}{\left(2\eta S_{in} + 2(1-\eta)S_{out}\right)^2} \\ w_{mut} &= \frac{1}{\left(2\eta S_{in} + 2(1-\eta)S_{out}\right)} \end{aligned} \tag{3.15}$$

Without a loss in generality, these weights can be scaled such that:

$$w_{in} + w_{out} + w_{mut} = 1 \tag{3.16}$$

3.4 Topological Level-Set

Thus the proposed methodology is as follows. At the start of optimization process (at a volume fraction of 1), suppose the mutual energy is small (this is usually the case), i.e., suppose:

$$\begin{aligned} w_{in} &\approx 0 \\ w_{out} &\approx 0 \\ w_{mut} &\approx 1 \end{aligned} \tag{3.17}$$

We then have:

$$\mathcal{T}_{\varphi} \approx \mathcal{T}_{mut} \tag{3.18}$$

In order to remove material, the key idea is to interpret the field $\mathcal{T}_{\varphi}$ as a level-set.

Specifically, Figure 7a illustrates the above field together with a cutting-plane at an arbitrary height τ that passes through the field. One can now define a domain Ω^{τ} per:

$$\Omega^{\tau} \equiv \{p \mid \mathcal{T}_{\varphi}(p) > \tau\}; \tau : \text{desired cutoff value} \tag{3.19}$$

In other words, the domain Ω^{τ} is the set of all points where the topological field exceeds τ; the induced domain Ω^{τ} is illustrated in Figure 7b. This corresponds to a topology of reduced volume fraction such that elements that contribute least to the objective are deleted. The cutting-plane value τ can be chosen such that, say, 5% of the volume is removed. This process however has to be repeated since the field problem has changed, and so have the topological sensitivity fields.

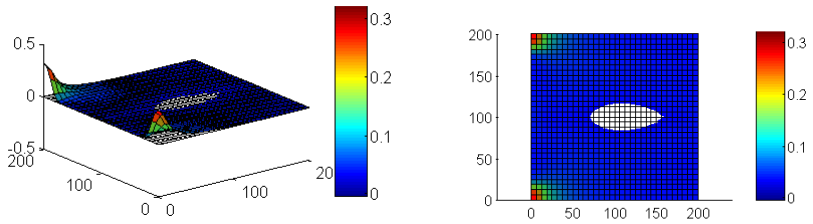

(a) Topological sensitivity field and a cutting plane. (b) Induced domain Ω^r

Figure 7: Topological sensitivity field for $w = (0,0,1)$.

For a desired volume fraction, a fixed-point iteration [36], [44], [45] is carried out involving three quantities (see Figure 8): (1) domain Ω^r, (2) displacement fields over Ω^r, and (3) topological sensitivity fields over Ω^r. Typically, 2~4 iterations are sufficient until convergence is reached in the objective. The fixed-point iteration is discussed in further detail, for example, in [36], [44], [45]. The concept of topological sensitivity has also been applied to stress-constrained volume minimization in [46].

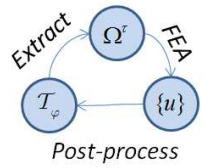

Figure 8: Fixed point iteration.

Once the volume fraction of 0.95 has been reached, the weights are recomputed using Equation (3.15). The process is repeated until the optimization cannot proceed further; see next Section for details.

4. IMPLEMENTATION

4.1 Finite Element Analysis

For finite element purposes, the spatial domain in 2-D is discretized into bi-linear quad elements (see Figure 9). In 3-D, tri-linear hexahedral elements are used since offer a good compromise between accuracy and speed. The corresponding shape-functions and element-stiffness matrices can be found in [47].

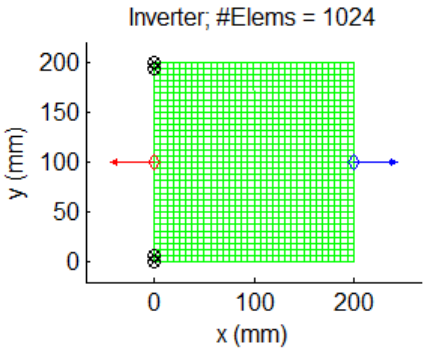

Figure 9: A finite element model with bilinear quad elements

When a topology is extracted using Equation (3.19), elements are classified as either being 'in' or 'out'; partial elements, i.e., pseudo-densities, are avoided here since they lead to stiffness matrices with large condition numbers [45], [48], and promote the formation of hinges. Thus, for example, after the first step of the optimization process, the domain may converge to the one illustrated in Figure 10.

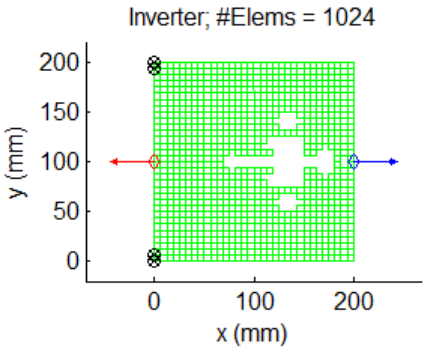

Figure 10: A new topology with reduced volume fraction.

Once a new topology is obtained, the element stiffness matrices of all the 'in-elements' are assembled to form the global K matrix. The input and output problems are then solved using the Jacobi-preconditioned conjugate gradient iterative solver. The reason for choosing an iterative solver over a direct solver is discussed in the next Section. Since pseudo-densities are avoided, the matrices are well-conditioned and the convergence is fast. Further, by avoiding pseudo-densities, many of the 'hinge-problems' [9] are avoided, as demonstrated through numerical experiments.

While the 'out-elements' are not included in the assembly of the global K matrix, these are allowed (and may) reenter during the next iteration as follows. Consider Figure 11a where the 'in' and 'out' elements within the current topology are identified; once the topological sensitivities over the 'in' elements are computed, the sensitivities at all nodes (see Figure 11b) are computed by averaging the element sensitivities. Finally, prior to the next iteration, an extrapolation procedure is implemented to predict the topological sensitivities over the 'out' elements that are adjacent to the boundary (see Figure 11c). This provides a mechanism for the 'out' elements to enter the optimization process (as observed in the numerical experiments), without having to assign pseudo-densities.

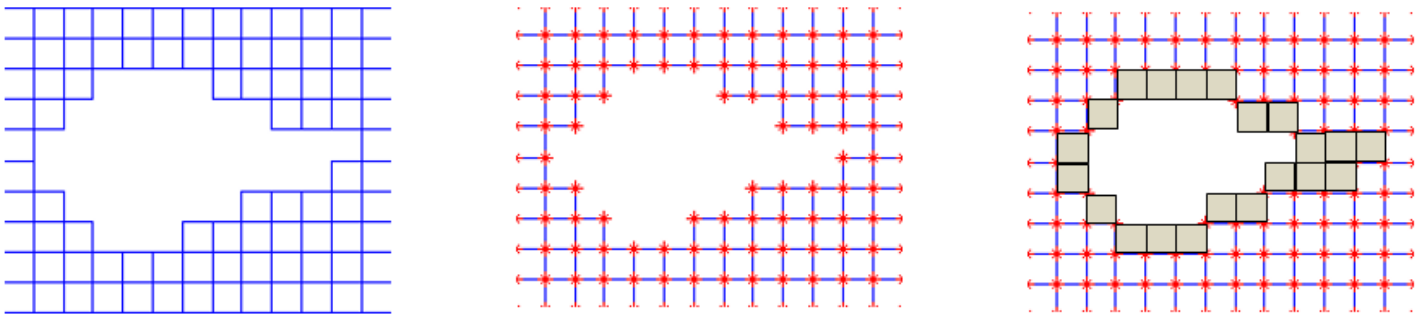

(a) Compute field over in-elements. (b) Estimate field over the nodes. (c) Estimate over 'out' elements near boundary.

Figure 11: Estimating the topological sensitivities over the 'out' elements

In 3-D, explicit assembly of large linear systems can be time and memory consuming. Therefore, in 3-D, we have chosen an 'assembly-free' (a.k.a. 'matrix-free') approach [49]. The linear system is solved using the *assembly-free* Jacobi-preconditioned conjugate-gradient method [50]. Since this only requires a sparse matrix-vector multiplication (SpMV), this is implemented as follows:

$$Ku = \left(\sum_e K_e \right) u = \sum_e K_e u_e \tag{3.20}$$

In other words, the element solution vectors are multiplied by the (non-zero) element stiffness matrices, and then assembled. An additional benefit of a matrix-free implementation is that only the non-zero elements need to be considered. As the topology evolves, the computational cost reduces dramatically.

4.2 Recovery from Pathological Cases

During the optimization process, certain pathological cases may arise. For example, one such case is illustrated in Figure 12 where the output force is disconnected. Fortunately, when an iterative solver is used, this can be easily detected since the residual error will grow rapidly, and the iterative solver can be terminated within a few iterations.

Once this condition is detected, the weights in Equation (3.16) are modified (in this instance, w_{out} is increased), and a new topology is extracted. The process is repeated until the finite element analysis is successful.

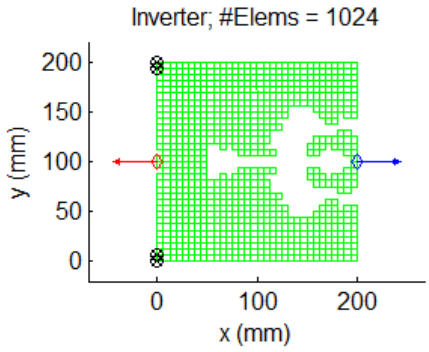

Figure 12: Pathological case of a disconnected mesh.

4.3 Algorithm

Thus the overall algorithm is as follows (see Figure 13):

1. We start with $\Omega^c = \Omega$, i.e., we start with a volume fraction of 1.0. The weights are computed per Equation (3.15)
2. A finite element analysis is carried out on Ω^c. The fields $\mathcal{T}_{in}, \mathcal{T}_{out}$ & $\mathcal{T}_{mut}$ are computed via Equations (3.11), (3.12) and (3.13). The level-set $\mathcal{T}_{\varphi}$ is computed via Equation (3.14). A simple filtering scheme is used where, at every node, the field is evaluated as the average of the field on all neighboring elements. Then, the field on every element is evaluated as the average of the field on all neighboring nodes.

3. Given the filtered level-set $\mathcal{T}_\varphi$ and a target volume fraction (typically 5% less than the current volume fraction), we seek the parameter τ such that the volume of Ω^τ is equal to the target volume fraction. This is a binary-search algorithm between the maximum and minimum values of $\mathcal{T}_\varphi$.

4. A fixed-point iteration is carried out on step-3 until the objective converges (to within a small percentage).

5. If the iteration fails to converge (due to pathological cases discussed above), the weights are modified as discussed previously. In particular, if the input-strain energy diverges then w_{in} is increased by a small amount (0.05), and if the output-strain energy diverges, then w_{out} is increased. The weights are then normalized per Equation (3.16) .

6. Once the above process converges to a specific volume fraction, the algorithm terminates if the final volume fraction is reached, or if w_{mut} is smaller than a prescribed value (0.1), i.e., no further reduction in volume fraction is possible.

7. (Else) The volume fraction is decreased and the weights are recomputed per Equation (3.15), and normalized per Equation (3.16).

8. Once the algorithm terminates, the iso-surface is extracted.

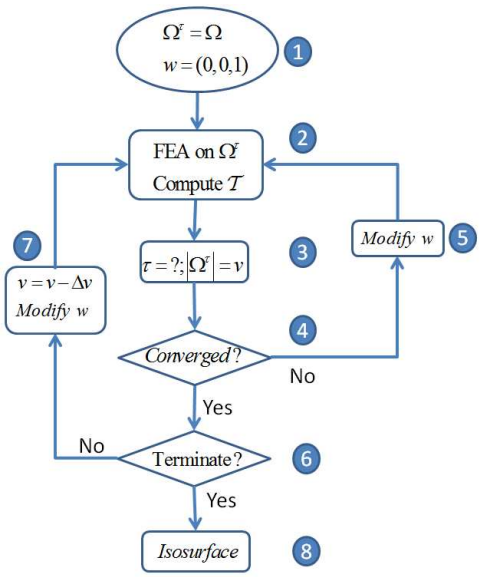

Figure 13: The proposed algorithm.

5. NUMERICAL EXPERIMENTS

In this Section, we present results from numerical experiments based on the above algorithm. Many of these examples have been analyzed in detail in [21]. Unless otherwise noted, the default parameters are:

- The material properties are that of Nylon with $E = 3GPa$ and $\nu = 0.4$.
- The volume step-size is 0.04.

- The target volume fraction is 0.005 (however, the algorithm may terminate at a larger volume fraction)
- The control variable η is set to 0.5.

The geometric and mechanical advantages are defined as:

$$GA \equiv \left. \frac{\text{Output displacement}}{\text{Input displacement}} \right|_{\text{Input force}} \tag{4.1}$$

$$MA \equiv \left. \frac{\text{Input displacement}}{\text{Output displacement}} \right|_{\text{Output force}} \tag{4.2}$$

All 2-D experiments were conducted sing Matlab R2013a running on a Windows 7 64-bit machine with the following hardware: Intel I7 960 CPU quad-core running at 3.2GHz with 6 GB of memory. The 3-D experiment was conducted using a C++ implementation with the following additional hardware: a graphics programmable unit (GPU) is an NVidia GeForce GTX 480 (480 cores) with 1.5 GB.

5.1 Inverter

The first example is that of an inverter. The finite element model is illustrated in Figure 14, where a domain of 200mm x 200mm is discretized with 1024 bilinear-quad elements. A force of 10 N is applied at (0,100), and an output in the opposite direction is desired at (200,100) as illustrated. The objective is to design a mechanism as light as possible, and the control parameter η is set to 0.5.

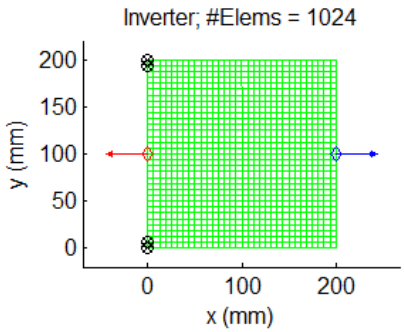

Figure 14: 2D finite element model for the inverter problem.

The algorithm terminated after 211 finite element operations, at a volume fraction of 0.205; see Figure 15. At termination:

- The displacement at the point of force application was 0.40 mm (to the left).
- The displacement at the output was 0.32 mm (to the right).
- The mechanism has a geometric advantage (GA) of 0.8 and a mechanical advantage (MA) of 0.71.
- These designs are topologically consistent with those found in the literature. However, the designs computed through the proposed method do not exhibit point-flexures.
- The time taken to compute the final design was approximately 2 minutes, 20 seconds.

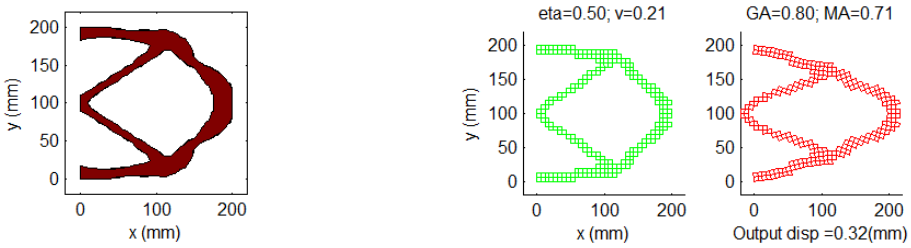

(a) Final design. (b) Un-deformed and deformed mesh.

Figure 15: The inverter design; deformation in (b) is scaled for clarity.

Observe the 'steady' increase in GA, MA and the objective as a function of the volume fraction in Figure 16.

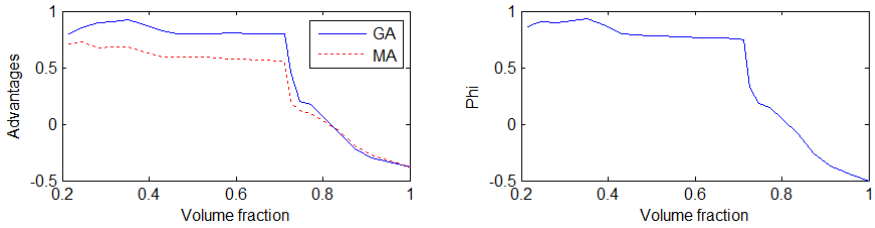

(a) Geometric and mechanical advantages. (b) Objective function φ

Figure 16: Mechanism history for the inverter.

Intermediate designs at volume fractions of 0.3 and 0.4 are illustrated in Figure 17.

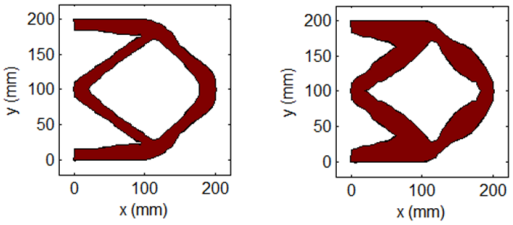

Figure 17: Intermediate designs for the inverter at volume fractions of 0.3 and 0.4.

5.2 Symmetric Inverter

Next consider the symmetric inverter posed in Figure 18 where the boundary is fixed on all four corners as illustrated; a force of 10 N is applied as shown.

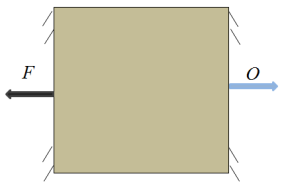

Figure 18: Symmetric inverter problem.

For a mesh discretization of 500 elements, the final design at a volume fraction of 0.29 is illustrated in Figure 19. The time taken is approximately 1 minute, 5 seconds. Once again, the designs are topologically consistent with those found in the literature, but do not exhibit point-flexures.

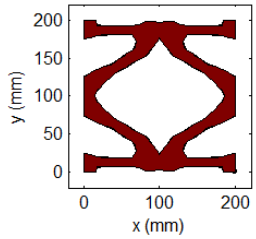

Figure 19: Symmetric inverter for 500 elements ($\eta = 0.5$).

As one can observe in Figure 20, due to the symmetry of the problem, the geometric and mechanical advantages are identical for all volume fractions.

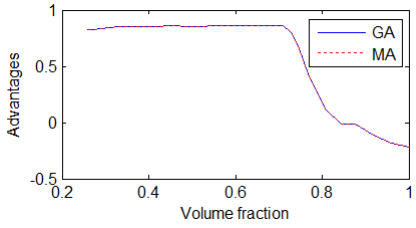

Figure 20: History of the geometric and mechanical advantages for the symmetric inverter.

To illustrate the mesh independency, the symmetric inverter for 1000 elements is illustrated in Figure 21.

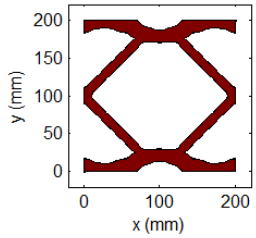

Figure 21: Symmetric inverter for 1000 elements.

5.3 Cruncher

Next consider the 'cruncher problem' posed in Figure 22'; two forces, each of 10 N is applied as shown. The objective here is to study the impact of the control parameter η ; the target volume fraction was set to 0.3.

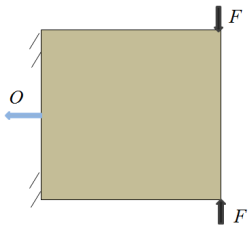

Figure 22: Cruncher problem.

For a mesh discretization of 1000 elements, and $\eta = 0.5$, the final design (devoid of point-flexures) is illustrated in Figure 23. The time taken is approximately 3 minutes, 15 seconds. As one can observe the geometric advantage of the mechanism if small (GA = 0.32), while the mechanical advantage is large (MA = 1.59).

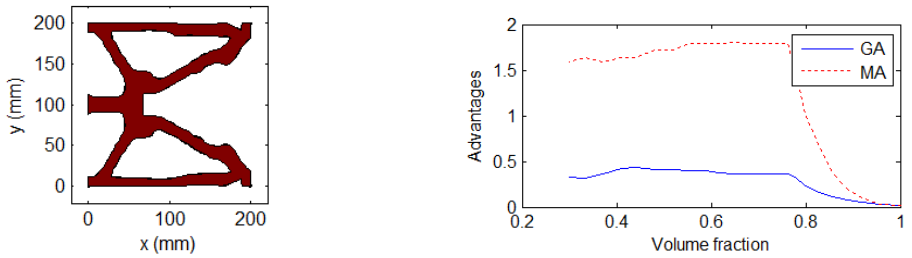

(a) Final design. (b) Geometric and mechanical advantages

Figure 23: Cruncher design for $\eta = 0.5$.

A simple method to increase geometric advantage (GA) is to increase the control parameter η. For $\eta = 0.6$, the design and results are illustrated in Figure 24. GA has increased to 0.59, while the mechanical advantage has dropped to 1.1. The time taken is approximately 3 minutes, 25 seconds. We avoid the extreme cases of $\eta = 0$ and $\eta = 1$, for the following reason. Consider the case of $\eta = 0$; observe that in Equation (3.15), the weight w_{in} vanishes. Thus, the corresponding topological sensitivity field $\mathcal{T}_{in}$ does not play a role during the optimization process, and therefore the topology will get disconnected from the fixed constraints on the left edge.

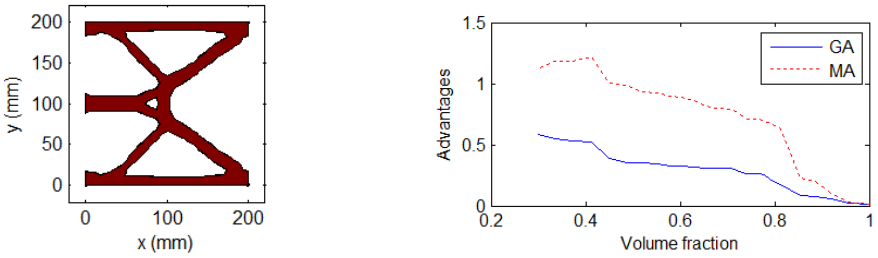

(a) Final design. (b) Geometric and mechanical advantages

Figure 24: Cruncher for $\eta = 0.6$

5.4 Grasper

Next consider the grasper problem posed in Figure 25; a force of 10 N is applied. Exploiting symmetry, only half the domain is modeled.

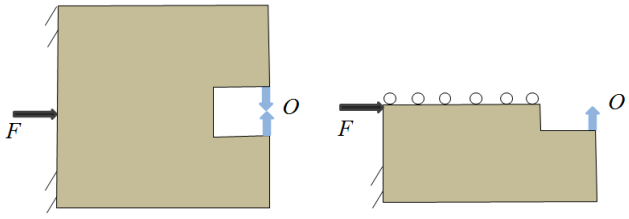

(a) Full model. (b) Model exploiting symmetry.

Figure 25: Grasper problem.

With a mesh discretization of 2000 elements, the final design (volume fraction of 0.3) is illustrated in Figure 26. With $\eta = 0.5$, the performance factors are: GA =0.62 and MA equal to 0.99.

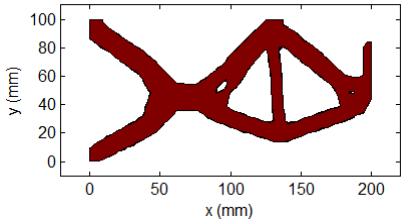

Figure 26: Grasper design.

5.5 Inverter (3-D)

The theory and algorithm extends to 3D, and is illustrated via a 3D inverter problem in Figure 27 where the dimensions of the domain are 200mm x 200mm x 10 mm. A force of 10 N is applied as shown, and an output in the opposite direction is desired as illustrated. The material properties are that of Nylon with $E = 3GPa$ and $\nu = 0.4$.

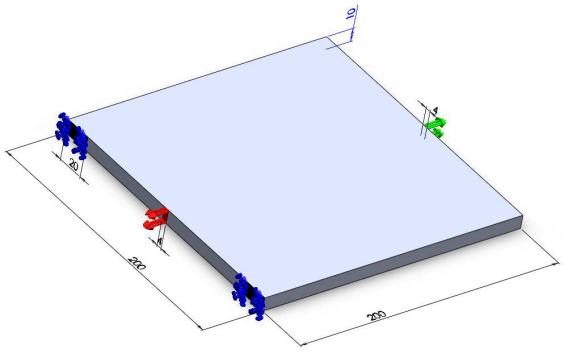

Figure 27: 3-D inverter problem.

The finite element model with 2000 tri-linear hexahedral elements is illustrated in Figure 28.

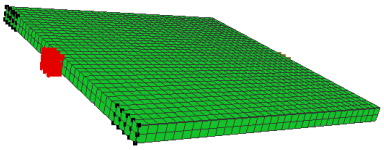

Figure 28: Finite element discretization with 2000 elements.

The algorithm terminated after 186 finite element operations, at a volume fraction of 0.20. The final design is similar to the 2-D version, with similar performance characteristics.

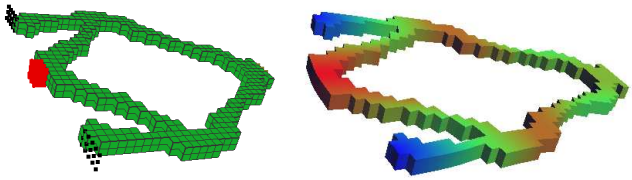

(a) Un-deformed (b) Deformed.

Figure 29: 3D inverter design.

5.6 Flap (3-D)

The final 3D example is that of a 'flap' whose dimensions are approximately 90 mm x 70mm x 10 mm. Other feature dimensions are as illustrated in Figure 30. On the back face, a force of 10 N is applied in the middle, and is fixed at the two ends. Output displacement is desired on the bottom face as illustrated; other flap designs have been considered in the literature [51].

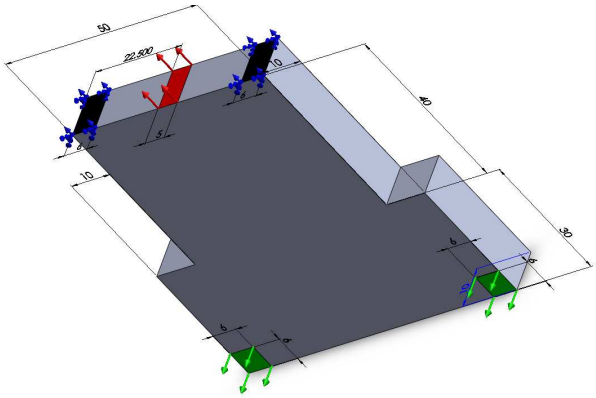

Figure 30: Flap problem.

The finite element model with 2000 tri-linear hexahedral elements was constructed and solved. The algorithm terminated after 246 finite element operations, at a volume fraction of 0.23 in 4 minutes. The performance factors are: GA = 1.1 and MA = 0.6.

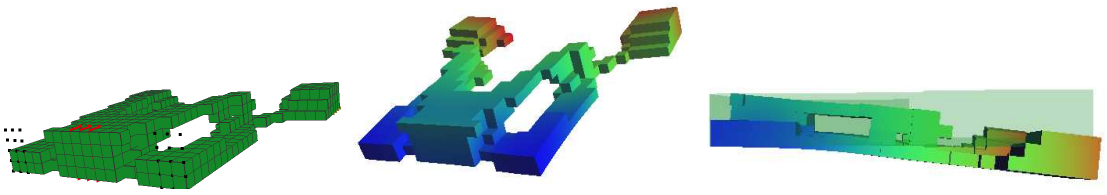

Figure 31: Flap design.

6. CONCLUSIONS

A new method for the topology optimization of compliant mechanisms was explored in this paper. The method relied heavily on the concept of topological sensitivity, and its viability was demonstrated through numerical experiments. Future work will focus on: (1) exploring design formulations that include springs and displacement/stress constraints, and (2) extending the current formulation to handle large deformation, and multi-physics.

Acknowledgements

The author would like to acknowledge NSF funding through grant CMMI-1232508 and CMMI-1161474; the author would also like to thank the reviewers, and Prof. G.K. Ananthasuresh (personal communication) for their valuable comments.

7. REFERENCES

[1] L. L. Howell, *Compliant Mechanisms*. New York: John Wiley & Sons, 2001.
[2] G. K. Ananthasuresh, S. Kota, and Y. Gianchandani, "A methodical approach to the design of compliant micromechanisms," in *Solid State Sensor and Actuator Workshop*, 1994, pp. 189–192.
[3] S. Kota, J. Joo, S. M. Rodgers, and J. Sniegowski, "Design of Compliant Mechanisms: Applications to MEMS," *Analog Integrated Circuits and Signal Processing*, vol. 29, pp. 7–15, 2001.
[4] S. Kota, K. J. Lu, Z. Kriener, B. Trease, J. Arenas, and J. Geiger, "Design and application of compliant mechanisms for surgical tools.," *J Biomech Eng*, vol. 127, no. 6, pp. 981–989, 2005.
[5] R. Ma, A. H. Slocum, E. Sung, J. F. Bean, and M. L. Culpepper, "Torque Measurement With Compliant Mechanisms," *Journal of Mechanical Design*, vol. 135, no. 3, p. 034502, 2013.
[6] G. K. Ananthasuresh and L. L. Howell, "Mechanical design of compliant microsystems—a perspective and prospects," *Journal of Mechanical Design*, vol. 127, no. 4, pp. 736–738, 2005.
[7] A. E. Albanesi, V. D. Fachinotti, and M. A. Pucheta, "A Review on Design Methods for Compliant Mechanisms," *Mecánica Computacional, Structural Mechanics (A)*, vol. XXIX, no. 3, pp. 59–72, 2010.
[8] L. Yin and G. K. Ananthasuresh, "Design of distributed compliant mechanisms," *Mechanics Based Design of Structures and Machines*, vol. 31, no. 2, pp. 151–179, 2003.
[9] E. L. Cardoso and J. Fonseca, "Strain energy maximization approach to the design of fully compliant mechanisms using topology optimization," *Latin American Journal of Solids and Structures*, vol. 1, no. 3, pp. 263–275, 2004.
[10] A. Saxena and G. K. Ananthasuresh, "On an optimal property of compliant topologies," *Structural and Multidisciplinary Optimization*, vol. 19, pp. 36–49, 2000.
[11] M. I. Frecker, G. K. Ananthasuresh, S. Nishiwaki, N. Kikuchi, and S. Kota, "Topological synthesis of compliant mechanisms using multi-criteria optimisation.," *Journal of Mechanical Design*, vol. 119, pp. 238–245, 1997.
[12] O. Sigmund, "On the Design of Compliant Mechanisms using Topology Optimization," *Journal of Structural Mechanics*, vol. 25, no. 4, pp. 494–524, 1997.
[13] M. Y. Wang and C. Shikui, "Compliant Mechanism Optimization: Analysis and Design with Intrinsic Characteristic Stiffness," *Mechanics Based Design of Structures and Machines: An International Journal*, vol. 37, no. 2, pp. 183–200, 2009.
[14] J. Lin, "A new multi-objective programming scheme for topology optimization of compliant mechanisms," *Structural and Multidisciplinary Optimization*, vol. 30, pp. 241–255, 2010.
[15] S. Rahmatalla and C. C. Swan, "Sparse monolithic compliant mechanisms using continuum structural topology optimization," *International Journal for Numerical Methods in Engineering*, vol. 62, pp. 1579–1605, 2005.
[16] R. Ansola, E. Vegueria, A. Maturana, and J. Canales, "3D compliant mechanisms synthesis by a finite element addition procedure," *Finite Elements in Analysis and Design*, vol. 46, pp. 760–769, 2010.
[17] Z. Luo, "Compliant mechanism design using multi-objective topology optimization scheme of continuum structures," *Structural and Multidisciplinary Optimization*, vol. 30, pp. 142–154, 2005.
[18] T. E. Bruns and D. A. Tortorelli, "Topology optimization of non-linear elastic structures and compliant mechanisms," *Computer Methods in Applied Mechanics and Engineering*, vol. 190, no. 26–27, pp. 3443–3459, 2001.

[19] G. Krishnan, C. Kim, and S. Kota, "A Metric to Evaluate and Synthesize Distributed Compliant Mechanisms," *Journal of Mechanical Design*, vol. 135, no. January, p. 011004, 2013.
[20] V. Mehta, M. Frecker, and G. A. Lesieutre, "Two-Step Design of Multicontact-Aided Cellular Compliant Mechanisms for Stress Relief," *Journal of Mechanical Design*, vol. 134, no. December, p. 121001, 2012.
[21] S. Deepak, M. Dinesh, D. Sahu, and G. K. Ananthasuresh, "A comparative study of the formulations and benchmark problems for topology optimization of compliant mechanisms," *Journal of Mechanisms and Robotics*, vol. 1, p. 011003, 2009.
[22] M. P. Bendsoe and O. Sigmund, *Topology Optimization: Theory, Methods and Application*, 2nd ed. Springer, 2003.
[23] G. I. N. Rozvany, "A critical review of established methods of structural topology optimization," *Structural and Multidisciplinary Optimization*, vol. 37, no. 3, pp. 217–237, 2009.
[24] J. A. Sethian, *Level set methods and fast marching methods*. Cambridge University Press, 1999.
[25] M. Y. Wang, S. K. Chen, X. M. Wang, and Y. L. Mei, "Design of multi-material compliant mechanisms using level set methods.," *Journal of Mechanical Design*, vol. 127, no. 5, pp. 941–956, 2005.
[26] T. Yamada, K. Izui, S. Nishiwaki, and A. Takezawa, "A topology optimization method based on the level set method incorporating a fictitious interface energy," *Comput. Methods Appl. Mech. Engrg*, vol. 199, no. 45–48, pp. 2876–2891, 2010.
[27] R. Ansola, E. Vegueria, J. Canales, and J. A. Tarrago, "A simple evolutionary topology optimization procedure for compliant mechanism design," *Finite Elements in Analysis and Design*, vol. 44, pp. 53–62, 2007.
[28] M. I. Frecker, N. Kikuchi, and S. Kota, "Topology optimization of compliant mechanisms with multiple outputs," *Structural and Multidisciplinary Optimization*, vol. 17, pp. 269–278, 1999.
[29] T. A. Poulsen, "A new scheme for imposing a minimum length scale in topology optimization," *International Journal for Numerical Methods.*, vol. 53, pp. 567–582, 2002.
[30] R. T. Shield and W. Prager, "Optimal structural design for given deflection," *J. Appl. Math. Phys*, vol. ZAMP21, pp. 513–523, 1970.
[31] H. A. Eschenauer, V. V. Kobelev, and A. Schumacher, "Bubble method for topology and shape optimization of structures," *Structural Optimization*, vol. 8, pp. 42–51, 1994.
[32] A. A. Novotny, R. A. Feijóo, C. Padra, and E. Taroco, "Topological Derivative for Linear Elastic Plate Bending Problems," *Control and Cybernetics*, vol. 34, no. 1, pp. 339–361, 2005.
[33] A. A. Novotny, R. A. Feijoo, and E. Taroco, "Topological Sensitivity Analysis for Three-dimensional Linear Elasticity Problem," *Computer Methods in Applied Mechanics and Engineering*, vol. 196, no. 41–44, pp. 4354–4364, 2007.
[34] A. A. Novotny, "Topological-Shape Sensitivity Method: Theory and Applications," *Solid Mechanics and its Applications*, vol. 137, pp. 469–478, 2006.
[35] J. Sokolowski and A. Zochowski, "On Topological Derivative in Shape Optimization," *SIAM journal on control and optimization*, vol. 37, no. 4, pp. 1251–1272, 1999.
[36] J. Céa, S. Garreau, P. Guillaume, and M. Masmoudi, "The shape and topological optimization connection," *Computer Methods in Applied Mechanics and Engineering*, vol. 188, no. 4, pp. 713–726, 2000.
[37] I. Turevsky, S. H. Gopalakrishnan, and K. Suresh, "An Efficient Numerical Method for Computing the Topological Sensitivity of Arbitrary Shaped Features in Plate Bending," *International Journal of Numerical Methods in Engineering*, vol. 79, pp. 1683–1702, 2009.
[38] I. Turevsky and K. Suresh, "Generalization of Topological Sensitivity and its Application to Defeaturing," in *ASME IDETC Conference*, Las Vegas, 2007.
[39] S. H. Gopalakrishnan and K. Suresh, "Feature Sensitivity: A Generalization of Topological Sensitivity," *Finite Elements in Analysis and Design*, vol. 44, no. 11, pp. 696–704, 2008.
[40] A. A. Novotny, R. A. Feijoo, E. Taroco, and C. Padra, "Topological Sensitivity Analysis," *Computer Methods in Applied Mechanics and Engineering*, vol. 192, no. 7–8Novo03, pp. 803–829, 2003.
[41] K. K. Choi and N. H. Kim, *Structural Sensitivity Analysis and Optimization I: Linear Systems*. New York: Springer, 2005.
[42] D. A. Tortorelli and W. Zixian, "A systematic approach to shape sensitivity analysis," *International Journal of Solids and Structures*, vol. 30, no. 9, pp. 1181–1212, 1993.
[43] R. A. Feijoo, A. A. Novotny, E. Taroco, and C. Padra, "The topological-shape sensitivity method in two-dimensional linear elasticity topology design," in *Applications of Computational Mechanics in Structures and Fluids*, CIMNE, 2005.
[44] J. A. Norato, M. P. Bendsøe, R. B. Haber, and D. A. Tortorelli, "A topological derivative method for topology optimization," *Structural and Multidisciplinary Optimization*, vol. 33, pp. 375–386, 2007.
[45] K. Suresh, "Efficient Generation of Large-Scale Pareto-Optimal Topologies," *Structural and Multidisciplinary Optimization*, vol. 47, no. 1, pp. 49–61, 2013.
[46] K. Suresh and M. Takalloozadeh, "Stress-Constrained Topology Optimization: A Topological Level-Set Approach," *Structural and Multidisciplinary Optimization*, vol. 48, no. 2, pp. 295–309, 2013.
[47] O. C. Zienkiewicz and R. L. Taylor, *The Finite Element Method for Solid and Structural Mechanics*. Elsevier, 2005.
[48] S. Wang, E. D. Sturler, and G. Paulino, "Large-scale topology optimization using preconditioned Krylov subspace methods with recycling," *International Journal for Numerical Methods in Engineering*, vol. 69, no. 12, pp. 2441–2468, 2007.
[49] C. E. Augarde, A. Ramage, and J. Staudacher, "An element-based displacement preconditioner for linear elasticity problems," *Computers and Structures*, vol. 84, no. 31–32, pp. 2306–2315, 2006.
[50] Y. Saad, *Iterative Methods for Sparse Linear Systems*. SIAM, 2003.
[51] B. Stanford and P. Beran, "Optimal Compliant Flapping Mechanism Topologies With Multiple Load Cases," *Journal of Mechanical Design*, vol. 134, no. May, p. 051007, 2102.

** The research was funded by the National Science Foundation (NSF)

LIST OF FIGURES